ELSEVIER

Journal of Power Sources 94 (2001) 230–237

JOURNAL OF POWER SOURCES

www.elsevier.com/locate/jpowsour

^{7}Li nuclear magnetic resonance study of lithium insertion in pristine and partially oxidized graphite

Y. Wang[a], V. Yufit[b], X. Guo[a], E. Peled[b], S. Greenbaum[a,*]

[a]*Physics Department, Hunter College of the City University of New York, 695 Park Avenue, New York, NY 10021, USA*
[b]*School of Chemistry, Tel Aviv University, Ramat Aviv 69978, Israel*

Received 28 July 2000; accepted 4 September 2000

Abstract

Pristine and partially oxidized graphite were lithiated electrochemically and investigated by solid state ^{7}Li nuclear magnetic resonance (NMR) methods. Both untreated and partially oxidized graphite exhibit three kinds of reversible Li sites, one, at an average position of 43 ppm for both stage 1 and 2 intercalation compounds (LiC_6 and LiC_{12}) at intermediate and higher lithiation levels, a stage 4 intercalation compound at 3 ppm (LiC_{24}), at low Li content, and Li associated with both edge sites and possibly stage 2L at intermediate Li content (at 11–13 ppm). The edge site population is enhanced in the partially oxidized graphite. Both treated and untreated graphite undergo reconstructive transitions in which the edge site lithium transforms into stage 1 intercalated lithium at higher levels of lithiation. Changes in both the NMR spectra and in the electrochemical parameters of stages 1, 2 and 4 have been noticed in the first two charge–discharge cycles. We attribute the changes in the NMR spectra and in the electrochemical parameters to graphite structural changes taking place in the first few cycles.

Keywords: Lithiated graphite; Lithium-7 NMR; Partially oxidized graphite

1. Introduction

The lithiated graphite anode, as a safe alternative to lithium metal, is a major factor in the commercial success of lithium ion batteries. The primary insertion mechanism of alkali metals into graphite is topotactic intercalation, which is a highly reversible reaction [1]. Of course the fact that this reaction can be induced electrochemically is the basis of its importance to battery technology. ^{7}Li nuclear magnetic resonance (NMR) has been shown to be a useful tool to investigate the local structural and electronic environment of intercalated Li ions. Since the first reported NMR study of lithium-intercalated graphite in 1977 [2], many papers on the subject have appeared [3–6]. The most important aspect of ^{7}Li NMR in this context is its sensitivity to the electronic environment of the Li^{+} ions. In particular, the stage 1 compound LiC_6 is metallic, which yields a relatively large Knight shift of the ^{7}Li resonance. Higher-stage compounds give different Knight shifts than that of stage 1. In addition, electrochemical decomposition of the electrolyte results in formation of a solid electrolyte interphase (SEI) on the surface of the carbon grains. The SEI consists of both inorganic (i.e. salts) and organic Li compounds that usually can be distinguished spectroscopically from intercalated Li. Moreover, NMR is a quantitative method by which the relative fractions of Li with different spectroscopic signatures can be determined in a straightforward manner.

Previous work by our group has shown that mild oxidation of graphite can improve its performance as a lithium ion battery anode material by increasing its reversible lithium capacity, decreasing its irreversible capacity and by facilitating the formation of a chemically bonded SEI [7,8].

2. Experimental

Natural graphite (NG7-Kansai Coke) was heated in air at 570°C for 30 min, resulting in up to an 8–10% mass reduction. Electrodes were prepared according to procedures described elsewhere [7,8]. Samples were electrochemically lithiated against lithium counter electrode in solution consisting of 1 M $LiAsF_6$ dissolved in ethylene carbonate diethyl carbonate 1:2 volume ratio with different values of x (as in Li_xC_6 corresponding to the nomenclature for Li-intercalated graphite) obtained during the first or the second deintercalation step. The cells were cycled on a

* Corresponding author. Tel.: +1-212-772-4973; fax: +1-212-772-5390.
E-mail address: steve.greenbaum@hunter.cuny.edu (S. Greenbaum).

0378-7753/01/$ – see front matter
PII: S0378-7753(00)00591-7

16-bit Maccor 2000 Battery Tester using the following procedure: the first discharge (intercalation) was carried out at 0.3 mA/cm^2 over the potential range of OCV to 0.2 V and at 50 μA/cm^2 over the voltage range 0.2–0.005 V. The charge steps and the consecutive discharge steps were carried out at 50 μA/cm^2 over the potential range 0.8–0.005 V. A higher current density was employed at the first intercalation step in order to minimize the irreversible capacity loss. Prior to sealing in Pyrex tubes under argon for NMR experiments, electrodes were washed in dimethyl carbonate and vacuum dried to remove any residual electrolyte salt. The electrode material was stripped from the Ni-screen current collector (for each sample), crushed and the dried powder was then packed into 5 mm OD Pyrex tubes and sealed under argon with Torseal, all procedures having been performed in an argon-filled glovebox.

NMR measurements were performed with a Chemagnetics CMX-300 spectrometer operating at a ^{7}Li resonance frequency of 117 MHz. Both wide-line and high resolution (MAS) spectra were obtained, the latter utilizing tightly fitting PTFE sleeves around the sealed sample tubes inside the MAS rotor, and spinning rates between 5 and 6 kHz. RF pulse widths corresponding to a 90° flip angle were about 4 μs. Aqueous LiCl solution was employed as a chemical shift reference. A sequence repeat delay of 20 s was employed for spectra acquisition in order to ensure complete relaxation of all spectral components. Spin-lattice relaxation times (T_1) were measured by inversion recovery.

Table 1
Lithiated pristine graphite

Sample	State	Li_xC (x=)
Y17 pristine	Cycle 2, charge	0.18
Y19 pristine	Cycle 2, charge	0.19–0.22
Y20 pristine	Cycle 2, charge	0.19–0.22
Y27 pristine	Cycle 2, charge	0.57
Y28 pristine	Cycle 2, charge	0.51
Y29 pristine	Cycle 2, charge	0.6
Y30 pristine	Cycle 2, charge	0.6

Table 2
Lithiated oxidized graphite

Sample (% burn off)	State	Li_xC (x=)
Y13 oxidized 8	Cycle 1, charge	0.42
Y14 oxidized 8	Cycle 1, charge	0.57
Y15 oxidized 8	Cycle 1, charge	0.18
Y16 oxidized 8	Cycle 1, charge	0.20
Y23 oxidized 9.5	Cycle 2, charge	0.47
Y24 oxidized 9.5	Cycle 2, charge	>0.7
Y25 oxidized 9.5	Cycle 2, charge	0.17
Y26 oxidized 9.5	Cycle 2, charge	0.17

3. Results

In this work, we found the differences of NMR spectra between lithiated pristine and oxidized graphite samples. As a result, we decided to look with greater detail into the electrochemical properties of the lithiated graphite during the two first intercalation–deintercalation cycles. The samples studied are listed in Tables 1 and 2. A typical charge–discharge curve (for sample Y26, Table 2) is depicted in Fig. 1. In a previous investigation, it was found that the *dQ*/*dV* curves of lithiated NG7 samples changed with graphite oxidation and with cycle number, and that these changes relaxed after two to three cycles [8]. Table 3 summarizes the following electrochemical parameters for the different stages: *dQ*/*dV* peaks for the intercalation (V_{int}) and deintercalation (V_{deint}) steps, pseudo equilibrium potential (E_r') values and the overpotential, η. E_r' values were calculated as the midvoltage between the intercalation and the deintercalation peaks. η was calculated as half the difference between V_{int} and V_{deint} assuming symmetric electrochemical behavior. Differences can be seen between cycle 1 and 2 and between oxidized and pristine samples for cycle 1. For all stages (1, 2, 4) in the first cycle partial oxidation does not affect V_{deint}, however, it slightly affects V_{int}. The difference in V_{int} between the pristine and oxidized samples increases with stage number; it is 4, 7 and 19 mV for stages 1, 2 and 4, respectively, where the oxidized samples have the lower values. Further justification for the stage 4 compound is given in the context of the NMR

Table 3
Intercalation and deintercalation voltages for pristine and oxidized NG7[a]

	Stage 1				Stage 2				Stage 4			
	V_{deint} (mV)	V_{int} (mV)	E_r' (mV)	η (mV)	V_{deint} (mV)	V_{int} (mV)	E_r' (mV)	η (mV)	V_{deint} (mV)	V_{int} (mV)	E_r' (mV)	η (mV)
First cycle												
Pristine	102 ± 5	77 ± 3	90 ± 4	25 ± 4	140 ± 4	109 ± 3	124 ± 3	31 ± 5	224 ± 3	192 ± 6	208 ± 4	31 ± 6
Oxidized	101 ± 1	74 ± 3	88 ± 1	27 ± 4	139 ± 1	102 ± 5	121 ± 2	37 ± 5	223 ± 2	173 ± 13	198 ± 7	49 ± 14
Second cycle												
Pristine	100 ± 2	80 ± 2	90 ± 2	20 ± 2	141 ± 3	114 ± 3	128 ± 4	26 ± 2	–	203 ± 3		–
Oxidized	98 ± 1	78 ± 1	89 ± 1	17 ± 2	137 ± 1	113 ± 2	125 ± 1	22 ± 3	–	204 ± 1		–

[a] Average for six samples.

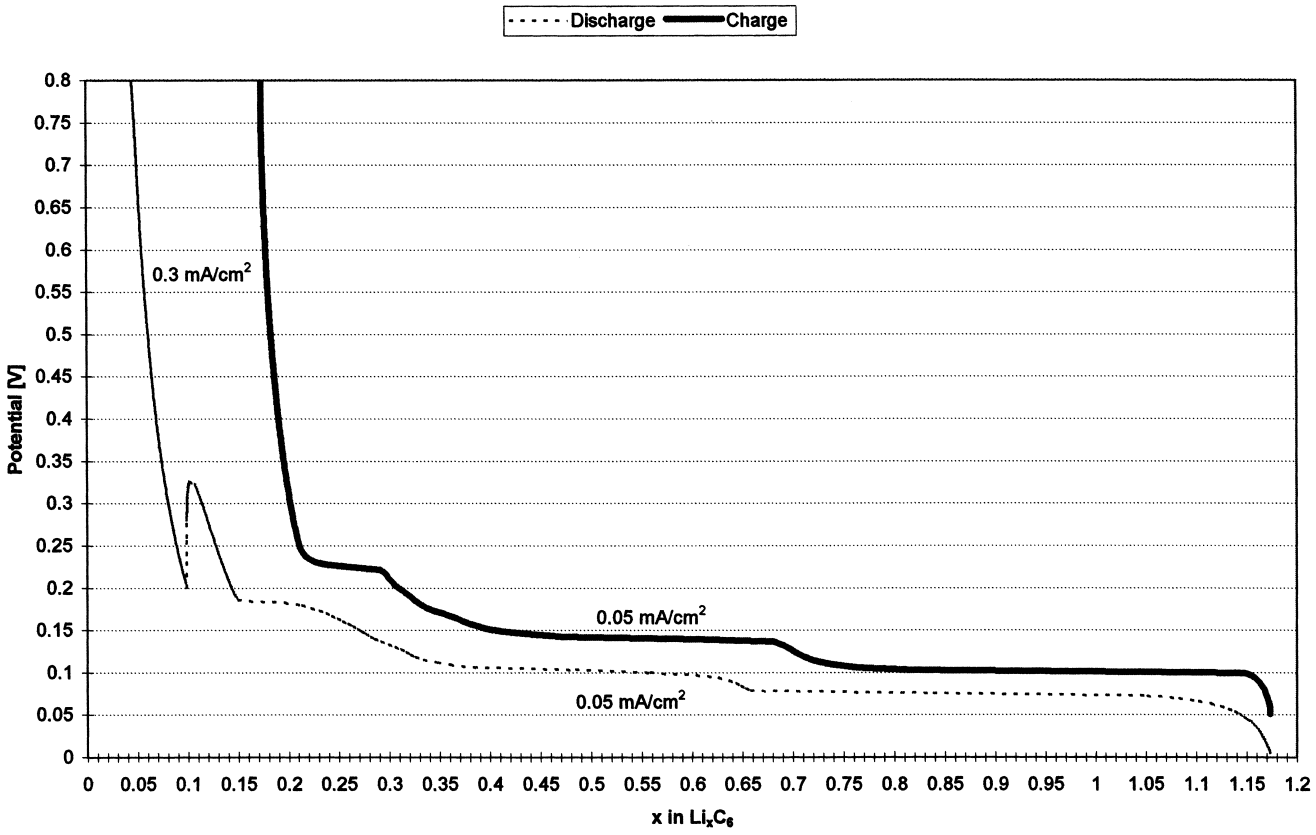

Fig. 1. Typical charge–discharge curve of partially oxidized natural graphite, in the first cycle (sample Y26, Table 2).

results later. Partial oxidation, in the first cycle, has a similar but smaller effect on E_r' (Table 3). In the first cycle η for the oxidized samples is higher than that of the pristine samples, this difference grows with the stage number. It is 2, 3 and 9 mV for stages 1, 2 and 4, respectively. In the second cycle, this difference disappears and in addition η is smaller. In the second cycle few other changes are seen: for all stages of both kinds of graphite, V_{int} moves to slightly higher values, there is almost no change in the position of V_{deint} and minor change in E_r' for stage 2. Although all these changes are small it is believed that they reflect a real trend, which may be correlated to changes in the NMR spectra discussed later.

In preparation of samples for NMR measurements the deintercalation process was stopped, either at the first or at the second cycle, at a predetermined x value. Tables 1 and 2 list, respectively, the pristine and partially oxidized graphite samples investigated in this work, including their calculated reversible lithium contents.

Wide-line ^{7}Li NMR spectra of lithiated pristine graphite, Li_xC_6, with x ranging from 0.18 to 0.60, are displayed in Fig. 2. Here, again, the relatively small amount of irreversible Li contained in the SEI is not included in the x-value. At low Li-content (up to $x = 0.22$) there is a single spectral component corresponding to a typical spin-3/2 powder pattern; i.e. a central transition and two satellite transitions.

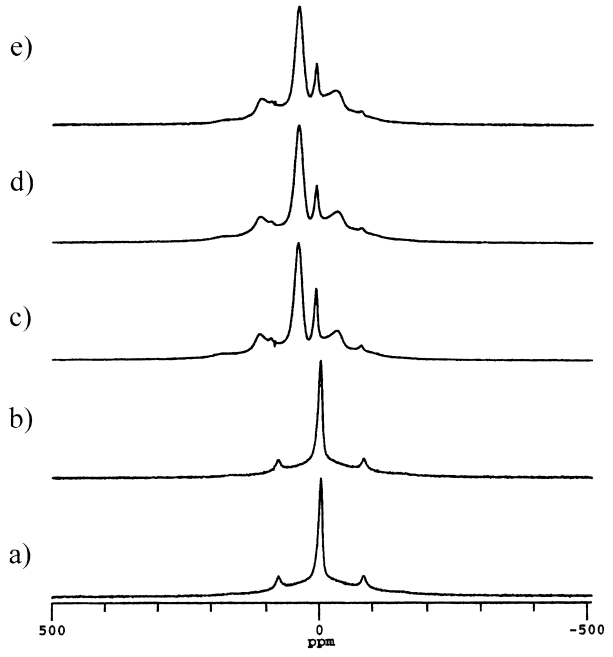

Fig. 2. Wide-line ^{7}Li NMR spectra of lithiated natural graphite. Sample designations are from Table 1. (a) $x = 0.18$ (Y17); (b) $x = 0.19$–0.22 (Y19); (c) $x = 0.51$ (Y28); (d) $x = 0.57$ (Y27); (e) $x = 0.60$ (Y30).

Table 4
NMR chemical shifts and quadrupole coupling constants of lithiated pristine graphite

Graphite pristine	Li_xC (x=)	Peak 1			Peak 2			Peak 3		
		Wide (ppm)	Spin (ppm)	e^2qQ/h (kHz)	Wide (ppm)	Spin (ppm)	e^2qQ/h (kHz)	Wide (ppm)	Spin (ppm)	e^2qQ/h (kHz)
Y17	0.18	2.5	3.8	36.8						
Y19	0.19–0.22	1.8	2.4	36.8						
Y20	0.19–0.22	1.1	2.7							
Y27	0.57		1.7		10.9	10.9	39.0	43.2	41.1	32.6
Y28	0.5l		1.0		11.3	11.0	39.0	44.0	41.2	33.0
Y29	0.6		2.7		10.9	10.2	39.2	43.9	41.5	32.8
Y30	0.6		1.1		11.0	10.6	39.0	43.6	41.2	32.8

From the latter separation, a quadrupole coupling constant (QCC) of about 37 kHz can be deduced. The peak of the central transition occurs at around 3 ppm (relative to aq. LiCl). Close examination of the spectrum reveals a slight asymmetry about the central transition peak, which is attributed to Li residing in the SEI at around 0 ppm. The spectra for $x = 0.51$, 0.57 and 0.60 are similar to each other in appearance, but dramatically different than those of the $x \sim 0.2$ spectra. The higher Li content samples exhibit two distinct Li sites, the dominant one with a central transition peak at 43 ppm and QCC of 33 kHz, and a smaller component with a central transition peak of 11 ppm and QCC of 39 kHz. The spectral parameters are summarized in Table 4. The 11 ppm feature exhibits its maximum intensity (not only relative to the other sites, but also absolutely) at $x = 0.51$ and decreases with further increased lithiation.

To assist in site assignment and analysis of their relative populations, high-resolution MAS measurements were performed (Fig. 3). For $x \sim 0.2$, the two bottom spectra in Fig. 3, only a single site is resolvable at 3 ppm, however with some asymmetry due, again, to a small component at 0 ppm from the SEI lithium. At higher Li content, it is possible to observe three sites, the SEI component at 0, 11 and the 43 ppm component. Although the SEI is not directly observable in the low Li content samples because of overlap with the 3 ppm signal, it can be resolved at low temperature by utilizing an inversion recovery pulse sequence in concert with MAS, as shown in Fig. 4. At -130°C, the difference in T_1 between the SEI Li and the 3 ppm feature, the latter with a longer T_1 than the former, results in selective inversion of the latter.

Wide-line ^{7}Li NMR spectra of oxidized graphite (8% burn-off) are displayed in Fig. 5. As in the case of pristine graphite, the lithiated oxidized graphite exhibits a single site for $x \sim 0.2$, with a central transition peak of 3 ppm and QCC of about 36 kHz. At higher lithiation, there are two dominant peaks, one at 13 ppm with QCC of 39 kHz, and one at 41–43 ppm with QCC of 33 kHz. This is, again, similar to the parameters noted for pristine graphite, except that the intensity of the 13 ppm peak in oxidized graphite is considerably larger than that of the 11 ppm feature in pristine graphite. Several spectra of lithiated oxidized graphite, with 9.5% burn-off, are displayed in Fig. 6. The spectral parameters corresponding to Figs. 5 and 6 are summarized in Table 5. In one of the samples at higher lithiation, there were the problems with that particular cell that prevented accurate determination of x. It is estimated that x is somewhat greater than 0.7 (but less than 0.8) in this sample. High-resolution MAS ^{7}Li spectra corresponding to the wide-line ones in Figs. 5 and 6 are shown in Figs. 7 and 8, respectively. From both Figs. 6 and 8 (spectra of 9.5% burn-off graphite), the SEI content is about the same as in the 8% burn-off material. This indicates that the formation of SEI is not strongly influenced by modest changes in the burn-off treatment. On the other hand, upon comparing SEI intensities with pristine graphite with a similar charging history, it is clear that the

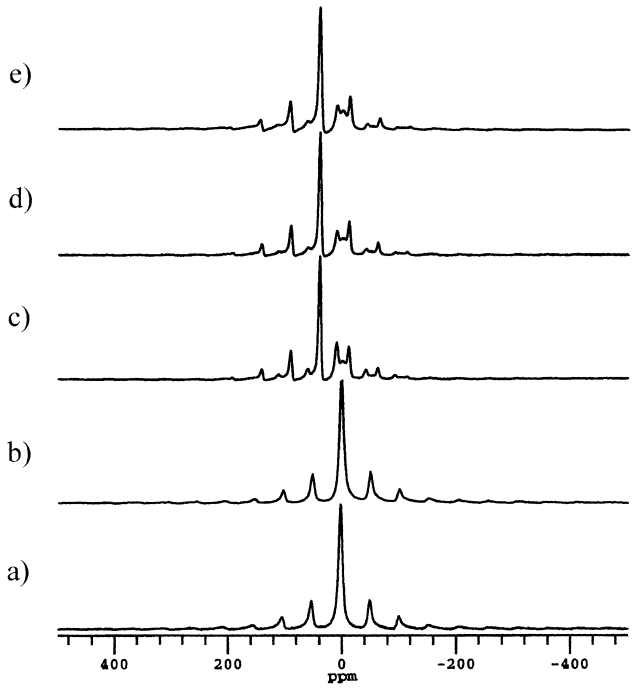

Fig. 3. High resolution MAS ^{7}Li NMR spectra of lithiated natural graphite. Sample designations are from Table 1. (a) $x = 0.18$ (Y17); (b) $x = 0.19$–0.22 (Y19); (c) $x = 0.51$ (Y28); (d) $x = 0.57$ (Y27); (e) $x = 0.60$ (Y30).

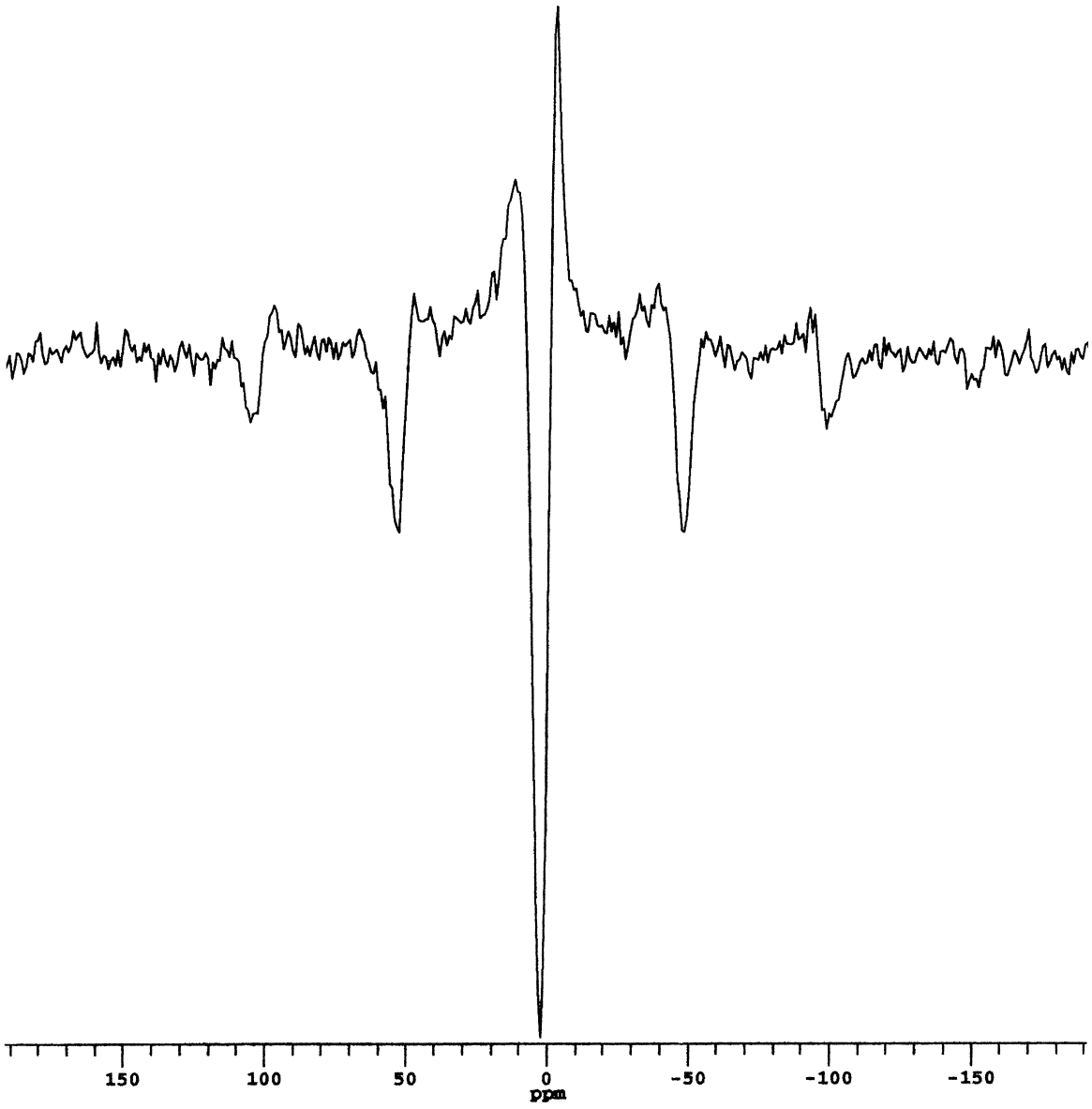

Fig. 4. Partially inverted ^{7}Li NMR spectrum of lithiated natural graphite at −130°C, illustrating different spin-lattice relaxation of 3 ppm feature and SEI.

Table 5
NMR chemical shifts and quadrupole coupling constants of lithiated oxidized graphite

Oxidized graphite burn-off (%)	Li_xC (x=)	Peak 1			Peak 2			Peak 3		
		Wide (ppm)	Spin (ppm)	e^2qQ/h (kHz)	Wide (ppm)	Spin (ppm)	e^2qQ/h (kHz)	Wide (ppm)	Spin (ppm)	e^2qQ/h (kHz)
Y13 8	0.42		3.7		10.5	13.3	39	43.2	43.5	33.2
Y14 8	0.57		2.5		9.7	13.3	39	41.3	42.8	33.2
Y15 8	0.18	1.4	3.8	36.4						
Y16 8	0.20	2.7	4.2	36.4						
Y23 9.5	0.47		1.8		10.2	12	39.4	43.2	42.2	33.0
Y24 9.5	0.7		1.6		11.0	11.4		42.5	42.0	33.6
Y25 9.5	0.17	0.4	2.1	35.8		10.4				
Y26 9.5	0.17	0.4	1.7	36?		12.3				

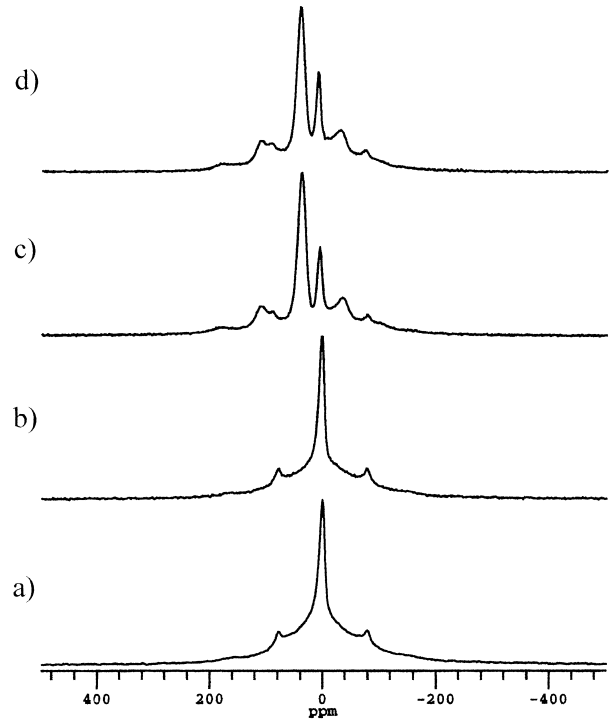

Fig. 5. Wide-line ^{7}Li NMR spectra of lithiated, partially oxidized (8% burn-off) natural graphite. Sample designations are from Table 2. (a) $x = 0.18$ (Y15); (b) $x = 0.20$ (Y16); (c) $x = 0.42$ (Y13); $x = 0.57$ (Y14).

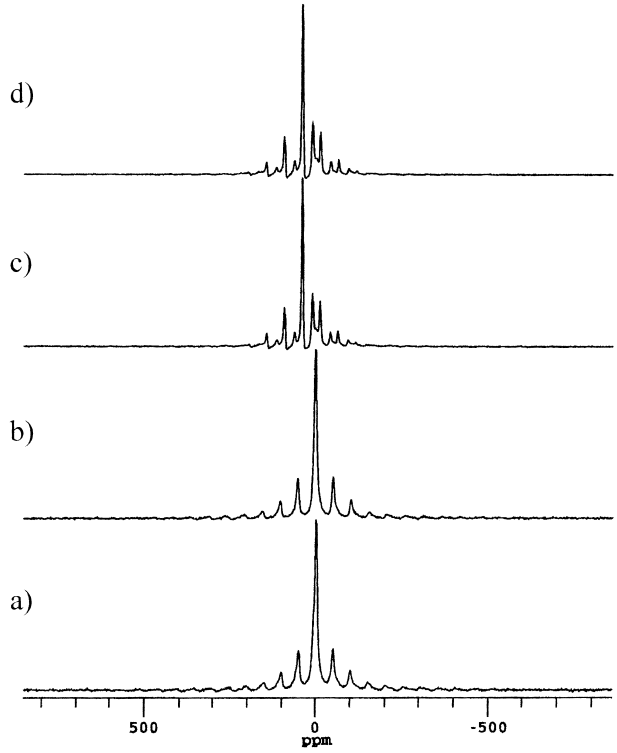

Fig. 7. High resolution MAS ^{7}Li NMR spectra of lithiated, partially oxidized (8% burn-off) natural graphite. Sample designations are from Table 2. (a) $x = 0.18$ (Y15); (b) $x = 0.20$ (Y16); (c) $x = 0.42$ (Y13); $x = 0.57$ (Y14).

oxidized samples exhibit a larger SEI component. This observation was reported in a previous study, which was attributed to a chemically-bonded SEI formed by electrochemically reaction with the partially oxidized graphite surface [8]. However, it was found that the irreversible capacity (Q_{ir}) is larger for the pristine samples. Combining this finding with the intensity data for peak 1 (3 ppm) leads to the conclusion that the SEI on the oxidized samples is richer in inorganic compounds like LiF or carbonates (and poorer in polymers) or that the formation process of the SEI

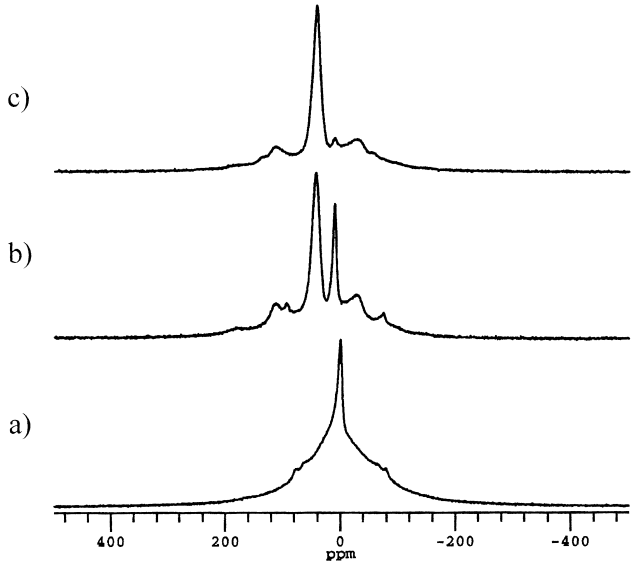

Fig. 6. Wide-line ^{7}Li NMR spectra of lithiated, partially oxidized (9.5% burn-off) natural graphite. Sample designations are from Table 2. (a) $x = 0.17$ (Y25); (b) $x = 0.47$ (Y23); (c) $x > 0.7$ (Y24).

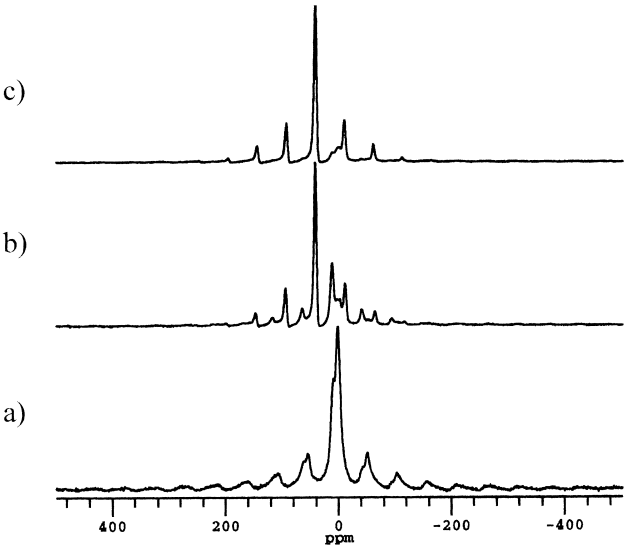

Fig. 8. High resolution MAS ^{7}Li NMR spectra of lithiated, partially oxidized (9.5% burn-off) natural graphite. Sample designations are from Table 2. (a) $x = 0.17$ (Y25); (b) $x = 0.47$ (Y23); (c) $x > 0.7$ (Y24).

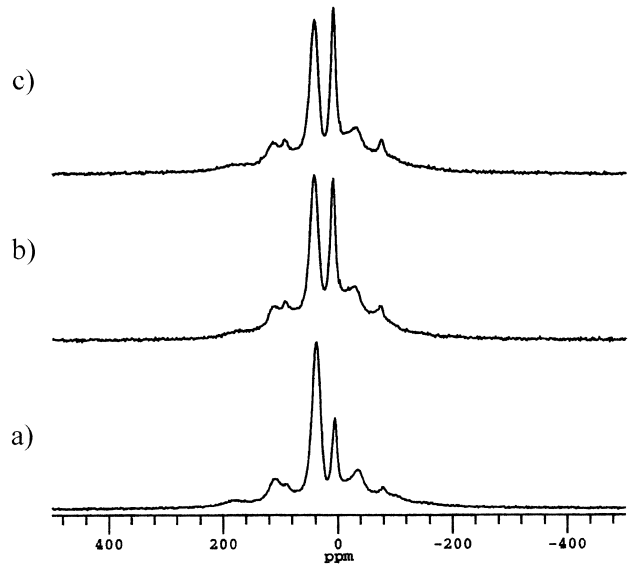

Fig. 9. Wide-line ^{7}Li NMR spectra of lithiated ($x = 0.42$), partially oxidized (8% burn-off) natural graphite, deliberately exposed to air.

is more efficient and requires less capacity. The spectral parameters of the lithiated-oxidized graphite are summarized in Table 5.

In an attempt to shed additional light on the nature of the 11(13) ppm peak in pristine (oxidized) graphite, wide-line NMR spectra of a deliberately air-exposed sample ($x = 0.42$ in 8% burn-off material) were obtained and are displayed in Fig. 9. It is clear that with increased air exposure, the 13 ppm (with QCC of 39 kHz) component increases in intensity. This suggests that this feature is a surface rather than intercalated site. A similar observation was made for the 11 ppm (39 kHz QCC) site in air-exposed lithiated pristine graphite.

4. Discussion

Careful analysis of the ^{7}Li chemical shifts (CS) presented in Tables 4 and 5 reveal slight differences between the first and the second intercalation deintercalation cycles and perhaps between the pristine and oxidized samples. The average CS for peak 1 of the pristine samples (Y19 and Y20, Table 4) after the first cycle is 2.6 ± 0.2 ppm; the one measured after the second cycle (Y27–Y30, Table 4) is lower, only 1.6 ± 0.6 ppm. Similar changes were found for peaks 1, 2 and 3 of the oxidized samples. The average CS values for peaks 1, 2 and 3 after the first cycle are 3.6 ± 0.5, 13.3 ± 0.0, and 43.2 ± 0.4, respectively (Y13–Y16, Table 5), the ones measured after the second cycle are lower, 1.8 ± 0.2, 11.5 ± 0.6, and 42.1 ± 0.1 ppm (Y23–Y26, Table 5). These CS changes correspond to changes in the dQ/dV curves, in η, and in the equilibrium voltage (Table 3). η values for the second cycle are smaller than those in the first one and E_r' values are slightly higher. We attribute the changes in the CS and in the electrochemical parameters to graphite structural changes taking place in the first few cycles. In order to formulate a coherent model of the mechanism of electrochemical lithium insertion in graphite, it is necessary to determine quantitatively the various site occupancies in addition to identifying the distinct Li sites. The results of this analysis are listed in Table 6, corresponding to MAS spectra. Spectral intensities of the various species are reported in Table 6 as a percentage of the total ^{7}Li NMR intensity of that particular sample. Wide-line spectra were also analyzed for consistency, and the modest disagreements in intensity distributions between the wide-line and MAS data are attributed to spectral overlap for the wide-line case, and incomplete accounting of spinning sideband intensities for the MAS case. In the case of strong spectral overlap between the SEI component near 0 and the 3 ppm feature, no attempt was made to resolve their relative intensities, except for having shown that they can be distinguished by selective inversion (Fig. 4). The 3 ppm (and 36 kHz QCC) signal appears at low levels of lithiation, and has been previously attributed to a high stage intercalation phase, such as LiC_{18} [6]. At higher Li content this phase is difficult to distinguish from the SEI and its corresponding quadrupole satellite transitions are unobservable. This is consistent with the conversion of high stage to low stage intercalated graphite as the lithium content increases. After detailed comparison of the peak intensity data in Table 6 with charge–discharge results, we conclude that the 3 ppm

Table 6
Relative spectral intensities based on MAS data

Graphite	Li_xC (x=)	NMR intensity of peak 1 <3 ppm (%)	NMR intensity of peak 2 <13 ppm (%)	NMR intensity of peak 3 <43 ppm (%)
Y14(O)	0.57	14	24	62
Y23(O)	0.47	19	22	59
Y24(O)	>0.7	12	2	86
Y25(O)	0.17	66	34	0
Y26(O)	0.17	76	24	0
Y27(P)	0.57	15	14	70
Y28(P)	0.51	9	23	68
Y29(P)	0.6	17	29	54
Y30(P)	0.6	18	12	70

peak is assigned to stage 4 intercalated graphite, i.e. to LiC_{24} and not to stage 3.

The 11 ppm feature is absent in pristine graphite at low lithiation ($x \sim 0.2$). Because of the unavailability of samples with $0.22 < x < 0.47$, it is impossible to tell precisely where (at what Li content) the onset of the 11 ppm feature occurs. However, it is clear that this site decreases in intensity with increasing lithiation. This is also observed in the case of oxidized graphite (note, in particular the very small 13 ppm component for the $x > 0.7$ sample in Figs. 6 and 8). On the other hand, close examination of oxidized graphite at low lithiation ($x \sim 0.2$) reveals a very small component at around 10–11 ppm which we believe is the same (or similar) site as that which gives rise to the 13 ppm feature at higher lithiation. On the basis of the increased intensity of this feature in oxidized compared to pristine graphite and its strong increase upon modest air exposure, we assign this spectral component to a surface-bonded, or edge site, rather than an interior or intercalated one. However, as its intensity is quite high we cannot exclude completely the possibility of some contribution from a stage 2L site, as described by Dahn and coworkers [9]. Zaghib and coworkers have assigned a similar 11 ppm (with 39 kHz QCC) site to a higher stage (stage 3) intercalated phase, and this would certainly account for its decrease with increasing lithiation, as has been stated above for the 3 ppm feature. However, as it did not disappear in samples with $x = 0.5-0.6$ and for the reasons cited above, having to do with factors that are expected to be more surface than bulk sensitive, we do not think that it relates to a higher stage. We believe that the 11(13) ppm feature in pristine (oxidized) graphite is mainly associated with a metastable edge site that is electrochemically reversible. On the basis of the charge–discharge behavior, due to the fact that the unlithiated graphite has (mostly) a ABAB packing, atomic-size voids exist between adjacent microphases (at the B edges). It is plausible that lithium atoms can reside at these sites. During the lithiation process (at higher x values) the graphite stacking changes to AAA and these edge sites are lost and the edge lithium ions move into the graphite galleries. The oxidized graphite has additional edge sites inside the nanosize voids created by the oxidation. The lithium at these sites may or may not move to the gallery at the end of the intercalation. Although the mechanism is unclear at the present time, lithium ions occupying this edge site seems to become intercalated into the structure at higher lithiation. The 43 ppm peak is assigned to both stage 2 (LiC_{12}) and stage 1 (LiC_6) intercalated graphite, both species having been shown to have very similar electronic environments and hence similar Knight shifts [2–6].

5. Conclusions

Electrochemically lithiated natural graphite in this study exhibits three reversible Li species — stages 1 and 2 intercalation compounds (LiC_6 and LiC_{12}, manifested by an average ^{7}Li Knight shift of 43 ppm, a 3 ppm feature assigned to a stage 4 compound (LiC_{24}), and Li bonded to edge sites with possible contribution of stage 2L (located at 11–13 ppm). The edge site occupancy is enhanced by partial oxidation of the graphite (up to 9.5% mass burn-off), and increasing lithiation results in host structural rearrangement which converts the edge-site Li into stage 1 intercalated Li.

Acknowledgements

This work was supported in part by grants from the United States Department of Energy, Division of Basic Energy Sciences, and the Israeli Ministry of Science. The authors would like to thank Kansai Coke for supplying the NG7 samples.

References

[1] M.S. Dresselhaus, G. Dresselhaus, Adv. Phys. 30 (1981) 139.
[2] J. Conard, H. Estrade, Mater. Sci. Eng. 31 (1977) 173.
[3] Y. Matsumura, S. Wang, J. Mondori, Carbon 33 (1995) 1457.
[4] K. Tatsumi, T. Akai, T. Imamura, K. Zaghib, Y. Sawada, J. Electrochem. Soc. 143 (1996) 1923.
[5] N. Imanishi, K. Kumai, H. Kokugan, Y. Takeda, O. Yamamoto, Solid State Ionics 107 (1998) 135.
[6] K. Zaghib, K. Tatsumi, Y. Sawada, S. Higuchi, H. Abe, T. Ohsaki, J. Electrochem. Soc. 146 (1999) 2784.
[7] E. Peled, C. Menachem, D. Bar-Tow, A. Melman, J. Electrochem. Soc. 143 (1996) L4.
[8] C. Menachem, Y. Wang, J. Flowers, E. Peled, S.G. Greenbaum, J. Power Sources 76 (1998) 180.
[9] J.R. Dalin, A.K. Sleigh. H. Shi, B.M. Way, W.J. Weydanz, J.N. Reimers, Q. Zhong, U. von Sacken, in: G. Pistoia, (Ed.), Lithium Batteries ——New Materials, Developments, and Perspectives, Elsevier, New York, 1994, p. 1.